High- and low-stress subduction zones recognized in the rock record

High- and low-stress subduction zones recognized in the rock record

Kazuhiko Ishii[1*] and Simon R. Wallis[2]

[1] *Department of Physical Science, Graduate School of Sciences, Osaka Prefecture University, Sakai, Osaka, Japan*

[2] *Department of Earth and Planetary Science, Faculty of Science, The University of Tokyo, Bunkyo-ku, Tokyo, Japan*

ABSTRACT

It is generally accepted that the main strength of subduction boundaries occurs in the shallower region where frictional deformation is dominant. However, estimates of absolute values—commonly expressed as apparent coefficient of friction, μ'—show great variation. Frictional shear heating is closely related to μ', and estimates of the extra thermal energy supplied by shearing can in principle be used to estimate subduction zone strength. One such approach is based on surface heat flow measurements. However, heat flow in convergent margins shows large local scatter and even in the same area, different studies using this method show large variations in estimates of μ' indicating large uncertainties. The thermal record of subduction conditions preserved in subduction-type metamorphic rocks is developed over geological time scales that average out local complexities in heat flow and therefore has good potential as an alternative indicator of the amount of shear heating and, hence, shear strength along subduction boundaries. Thermal models that incorporate shear heating were developed for two contrasting and well-known subduction-type metamorphic belts: the relatively warm Sanbagawa belt of SW Japan and the relatively cold Franciscan belt of western USA. High-grade rocks of the Sanbagawa belt show strongly curved *P–T* paths that display increasing *P/T* to about 2 GPa. Information on the rate of plate movement and the age of the subducting slab at the time of metamorphism can be combined with modelling results to show that relatively high shear stresses, equivalent to $\mu' \sim 0.13$ are required to account for the observed curved *P–T* paths. In contrast, the high-grade rocks of the Franciscan belt show relatively cool *P–T* conditions that do not allow for strong shear heating with an appropriate upper bound for μ' of ~0.03. Modelling suggests subduction rate and lithology are potentially important controls on the development of high- versus low-stress subduction zones. High-stress subduction zones are likely to be associated with high aseismic/seismic slip ratios possibly related to slab roughness.

Keywords: subduction boundary, shear stress, Sanbagawa belt, Franciscan belt, numerical model, metamorphic *P–T* paths

* Corresponding author at: Department of Physical Science, Graduate School of Sciences, Osaka Prefecture University, Gakuen-cho, Sakai, Osaka, 599-8531, Japan.
E-mail addresses: ishii@p.s.osakafu-u.ac.jp (K. Ishii).

1. Introduction

Knowledge of the strength of subduction plate boundaries is an essential part of understanding the conditions necessary for plate tectonics, the processes leading to great earthquakes that occur along subduction megathrusts and the thermal structure of subduction zones. At relatively shallow levels, deformation along subduction boundaries is dominated by brittle processes that can be modelled as frictional behaviour and the strength increases in proportion to the normal stresses acting across the boundary. This frictional domain broadly corresponds to the seismogenic zone. At greater depths, increased pressure and temperature favour non-frictional ductile deformation by crystal plastic processes and a decrease in strength and shear stresses. The main strength of the subduction boundary is in the frictional domain. This strength can be conveniently expressed by using the ratio of shear to normal stress known as the coefficient of friction, μ, or the apparent coefficient, μ', when the effects of fluid pressure are taken into account. Previous studies of subduction boundaries using force balance (Lamb, 2006) or heat flow (Gao and Wang, 2014; England, 2018) arguments yield estimates of μ' ranging from 0.02 to 0.13 (Fig. 1). An alternative approach using a global 3D thermo-mechanical model (Osei Tutu et al., 2018) requires the average μ' along plate boundaries to be ≤ 0.05 to match the observed present-day plate motion and net rotation. In contrast to these estimates, laboratory rock deformation experiments at non-seismic slip rates summarized as Byerlee's Law yield values of μ' ~ 0.4, assuming hydrostatic fluid pressure.

The above summary shows that the range of available estimates for the strength of subduction zones and associated stresses vary over an order of magnitude. In some cases application of very similar approaches by different workers leads to very different results even in the same location, e.g. in the northern Hikuragi subduction margin (Fig. 1). Therefore, it is desirable to investigate alternative approaches to this problem. Here, we show how studies from some types of subduction-type metamorphic rocks can be used to estimate the strength of ancient subduction zones.

Slip along major faults such as subduction boundaries produces heating that depends on the shear stress and slip velocity. Therefore, information about the thermal budget of subduction zones has potential to be used as an indicator of shear stress; one useful source of information is the surface heat flow. A difficulty encountered when using surface heat flow is its strong local scatter due to the influence of localized fluid flow and other upper crustal processes. A more direct record of the thermal structure close to subduction boundaries is found in subduction-type metamorphic rocks. This metamorphic record is developed over time scales of millions of years and will be largely unaffected by short-term fluctuations making it potentially a more robust indicator of shear stress in subduction zones than surface heat flow. The pioneering work by Peacock (1992) uses a combination of analytical and numerical models combined with estimates of metamorphic conditions of blueschist-facies metamorphism to constrain possible amounts of shear heating with an emphasis on conditions recorded in the Franciscan belt. Peacock (1992) deduces a range of μ' of ~0–0.14. However, a more detailed discussion was hampered by a lack of good constraints on important variables such as the age of subducting oceanic plate, subduction rate and elapsed time after subduction initiation.

The past 25 years have seen major advances in numerical modelling of subduction zones, understanding of the rheology of subduction-related rocks and a great increase in the amount and precision of the information that is needed to model examples of ancient metamorphism. These advances mean it is now timely to revisit the idea of combining thermal modelling with studies of individual subduction-type metamorphic belts to constrain shear stresses along subduction boundaries. Here, we present a thermal model for subduction zones that incorporates shear heating based on recent summaries of fault rock rheology and investigate the implications for stresses in two contrasting domains of subduction-type metamorphism: the relatively warm Sanbagawa belt in SW Japan and the relatively cool Franciscan belt in W USA.

2. Thermal model

Our two-dimensional model consists of a kinematically prescribed subducting slab (including a 7 km thick oceanic crust), a viscous mantle wedge with temperature- and stress-dependent rheology, and an overriding rigid 'lithosphere' (Fig. 2A). This overriding 'lithosphere' consists of 15 km of upper continental crust and 15 km of lower continental crust for continental lithosphere and 10 km of oceanic crust and 20 km of mantle for oceanic lithosphere. The governing equations for the flow and temperature fields are the conservation equations of mass, momentum, and energy, with the extended Boussinesq approximation (see Appendix A). The analysis uses the code I2VIS (Gerya and Yuen, 2003), which is based on finite differences with a marker-in-cell technique and a fully staggered rectangular Eulerian grid. The model domain (200 km deep × 443 km wide) includes a 200 × 200 grid and ca 3.2 × 10^6 markers.

In common with other geodynamic models of subduction zones, we assume that beyond a certain critical depth there is complete viscous coupling between the subducting slab and the overriding mantle that drives flow in the wedge. In contrast, at relatively shallow depths, we assume the slab and the wedge mantle are decoupled over geological time scales; this approach also follows previous studies (e.g. Wada and Wang, 2009). The transition from a decoupled to a coupled interface occurs at a depth of 70–80 km irrespective of subduction zone (Wada and Wang, 2009). The variable Dc is used to denote the down-dip limit of full decoupling. We use a velocity boundary condition along the slab-wedge interface: no coupling ($v = 0$) for depths < Dc and complete coupling ($v = vs \cos\phi$) at depths > Dc + 10 km, with a transitional zone over the intervening 10 km depth range. vs is the subduction rate and ϕ is the angle of obliquity with respect to the subduction boundary such that $vs \cos\phi$ is the trench normal component of subduction velocity. The bottom of the overriding rigid 'lithosphere' forms the top boundary of the wedge ($v = 0$). The back-arc vertical boundary of the mantle wedge is treated as a stress-free ($\sigma_{xx} = 0$) inflow/outflow boundary (Fig. 2A).

The left-side thermal boundary condition is the oceanic geotherm for a given plate age corrected for the subduction angle and calculated using a plate cooling model with a 95 km plate thickness and T = 1450 °C at the plate base (Stein and Stein, 1992). The temperatures of the oceanic asthenosphere are calculated using an adiabatic temperature gradient of 0.3 °C/km. The thermal structure of the overriding plate is used as the initial temperature distribution (Fig. 2B). The thermal boundary condition used for the right-side inflow boundary is either an oceanic or continental thermal structure depending on the type of overriding plate. For each step in the calculation, the temperature gradients normal to the boundaries, dT/dz and dT/dx, from the previous step are applied to the bottom and right-side outflow boundaries, respectively. The top surface has a constant temperature of 0 °C (Fig. 2A). The continental geotherm is based on a 1D steady-state conduction model incorporating radiogenic heat production that yields a surface heat flow of 75 mW/m^2. The deeper part (> 67 km) is assigned a geotherm calculated assuming a mantle potential temperature of 1300 °C and an adiabatic temperature gradient of 0.3 °C/km.

To incorporate the shear stress along the decoupled and partially decoupled subduction boundary, τ, we use a combination of frictional stress τ^F and viscous flow stress τ^V following Noda and Shimamoto (2012) and Gao and Wang (2014),

$$\tau = \tau^V \tanh\left(\frac{\tau^F}{\tau^V}\right). \qquad (1)$$

The shallow part of the boundary is governed by the static friction law

$$\tau^F = \mu(\sigma_n - p_f) = \mu(1-\lambda)\sigma_n = \mu'\sigma_n \qquad (2)$$

where λ is the ratio of fluid pressure p_f to normal stress σ_n (approximately the weight of the overlying rock column), so that the apparent coefficient of friction μ' includes contributions from both the intrinsic friction μ and pore-fluid pressure p_f. The deeper part of the boundary is assumed to follow the flow law for quartz (Luan and Paterson, 1992; Evans and Kohlstedt, 1995)

$$\tau^V = f\ \left(\frac{1}{A}\frac{vs}{w}\right)^{\frac{1}{n}} \exp\left(\frac{E}{nRT}\right), \qquad (3)$$

where n = 3.1 and $A = 10^{-7.18}$ /(MPa^n s) are experimentally determined parameters, E = 135 kJ/mol is the activation enthalpy, w (= 300 m) is the thickness of the shear zone that accommodates fault slip and f is a scaling factor for τ^V. The material in the subduction boundary zone, or channel will comprise several different lithologies. To model such variation directly would require incorporating multiple flow law parameters with different values that reflect variations in mineralogy, flow mechanism, and/or grain size. For our purposes a simpler approach is sufficient, and we employ a single parameter, f, to investigate possible variations in viscous stresses. The rate of heat dissipation per unit fault area H_f is expressed by

$$H_f = \tau\ vs. \qquad (4)$$

3. Model results

The temperature distribution along the subduction boundary varies with the age of the subducting plate (*age*), subduction rate (*vs*) and apparent coefficient of friction (μ’) (Fig. 3A). All *P–T* profiles show a rapid increase in temperature at ~2.4 GPa, which corresponds to the coupling depth *Dc* between slab and mantle wedge (Figs. 3A, C). Subduction-type metamorphic rocks do not generally return from depths greater than 80–90 km, and we focus on the part of the subduction boundary at depths shallower than *Dc*. For this depth range and for zero frictional heating (μ’ = 0), a younger plate age and a slower subduction rate (i.e. smaller advective cooling) results in higher temperatures. For non-zero values of μ’, the effect of frictional heating is larger for higher subduction rates and older, i.e. colder, plates. As an example, for a slab with *age* = 100 Ma and a subduction velocity, *vs*, of 10 cm/yr, the temperature along the subduction boundary in the 1–2 GPa pressure range for μ' = 0.1 is ca 350 ºC higher than for μ' = 0. In contrast, for a slab with an *age* = 10 Ma and *vs* = 3 cm/yr, the difference in temperature is less than 100 ºC. In addition to the direct relationship between the slip rate and frictional heating (Equation 4), the temperature along the subduction boundary is also affected by the temperature- (related to both *age* and *vs*) and slip-rate dependence of the viscous shear stress (Equation 3). For the case of *age* = 10 Ma and *vs* = 3 cm/yr, the low viscous stresses are due in part to the overall high T caused by subduction of a young warm plate. The relatively slow subduction rate also limits the viscous shear stresses firstly by keeping the rocks relatively warm due to limited subduction-related advective cooling and secondly by maintaining a low strain rate (vs/w). Low viscous stresses tend to restrict the range of the frictional fault zone that produces most of the shear heating. The net result is low average stress and low shear heating even for a relatively high μ' value of 0.1 (Fig. 3B). In contrast, for the same value of μ' = 0.1 but with *age* = 100 Ma and *vs* = 10 cm/yr the overall reduction in temperature and the higher strain rate (vs/w) results in higher viscous stress and strong shear heating, in both the frictional and viscous domains, with temperatures ~500 ºC at $P > 1$ GPa. Even at these elevated temperatures the viscous shear stresses are high due to the effect of the velocity-strengthening nature of the viscous rheology.

An important feature shown by our and previous modelling is that shear stress—and hence also shear heating—along the boundary reaches a maximum at shallower depths for higher μ' (Fig. 3B). One of the implications of this stress distribution is that for μ' greater than about 0.1, the P–T profile shows a strong upwardly concave shape with an increasing P/T slope reaching a maximum close to ~2 GPa (Fig. 3A). This feature of the thermal structure and P–T paths of metamorphic rocks has the potential to be used as a marker of high-stress subduction. A second important feature is that in the pressure range of 1–2 GPa and for μ' values larger than 0.1, the temperature along the subduction boundary shows only slight changes for increases of μ’. A particular characteristic feature of high stress models—those with relatively large values of μ’—is the presence of a high *T* zone close to the subduction boundary at depths of 20–40 km (Fig. 3C). A similar feature is also seen in other published models (Gao and Wang, 2014).

The above results show that with the exception of young and slowly subducting slabs, increasing the shear strength (expressed as μ’) of the subduction boundary from 0 to 0.2 can result in major changes in the shape of expected *P–T* paths of subducted rocks and temperature rises up to several hundreds of degrees. These differences are large enough to be recognized in metamorphic rocks offering a potential way to estimate shear stresses from petrological studies of *P–T* conditions along the ancient subduction boundaries.

4. Comparison with subduction metamorphic belts

4.1. Sanbagawa belt

The Sanbagawa belt of SW Japan is a well-documented example of oceanic subduction metamorphism (e.g. Wallis and Okudaira, 2016) lacking subsequent continental collision and showing good preservation of subduction features. The age of the main phase of metamorphism is well constrained by Lu–Hf dating of eclogite (Wallis et al., 2009) at around 89 Ma. Confirmation of this age is given by the presence of detrital zircon U–Pb ages as young as ~90 Ma and K–Ar and Ar–Ar mica ages in the range of 85–70 Ma (Knittel et al., 2014; Aoki et al., 2019, Wallis and Okudaira, 2016 and references therein). These represent pre-metamorphic protolith ages and post-peak metamorphism cooling ages and should therefore bracket the peak metamorphic age. Locally there are older domains that show subduction metamorphism at around 120 Ma (Endo et al., 2009; Okamoto et al., 2004). A shallow *P*/*T* slope developed at 116 Ma (Fig. 5A) followed by cooling—commonly described as an anticlockwise *P*–*T* path—implies these formed shortly after the onset of subduction (Endo et al., 2009) and are distinct from the main phase of metamorphism.

The mid to late Cretaceous age of the Sanbagawa metamorphism restricts the possible plates that could have been responsible for the Sanbagawa subduction. In addition, kinematic studies show the plate motion vector was oblique to the east Asian continental margin and associated with sinistral shear (Wallis et al., 2009). Together these features show the Izanagi plate can be confidently identified as the plate that caused the Sanbagawa metamorphism. Plate reconstructions for this period show convergence of the Izanagi Plate with east Asia was unusually rapid (20–24 cm/yr) with an obliquity of ~30º (Engebretson et al., 1985; Wallis et al., 2009; Müller, et al., 2016).

Another important input parameter for the modelling is the age of the subducting slab. The relatively warm metamorphic conditions of the Sanbagawa belt have led several workers to suggest the age of the slab was young (Aoya et al., 2003). However, recent plate constructions suggest an age of around 60 Ma (Müller, et al., 2016). An age around 60 Ma at the time of subduction has been confirmed by recent dating. Re–Os dating of sulphide ore minerals in samples of numerous Besshi-type Cu deposits of the Sanbagawa belt (Nozaki et al., 2013) yield ~150 Ma ages. These deposits are thought to form by sea floor hydrothermal processes close to an active spreading ridge. The difference in the ages of ore genesis close to a spreading ridge (~150 Ma) and of peak metamorphism shortly after the slab enters the subduction zone (~90 Ma) gives a slab age close to 60 Ma at the time of subduction. It is possible that the Besshi-type deposits formed by off-axis activity. However, this would imply a greater age for the slab and not younger, and the thermal structure for slabs older than about 60 Ma shows little change.

In addition to the above constraints on the slab subduction rate and age, in our modelling we also use (i) the time since initiation of subduction, based on the 30 million year age difference between the onset of subduction around 120 Ma and the main recorded metamorphism at 90 Ma, and (ii) a continental geotherm for the overlying plate, based on the configuration before the opening of the Sea of Japan (Maruyama et al. 1997). The Sanbagawa belt consists of a series of stacked sheets of ~1 km thickness (e.g. Wallis and Aoya, 2000) and in our modelling we also examine the thermal structure in a suitable domain below the subduction boundary.

We now use the above boundary and initial conditions to model the thermal evolution of the Sanbagawa subduction zone and compare the results for different amounts of shear heating with the *P–T* conditions recorded by the metamorphic rocks. We focus on the subduction-related *P–T* paths up to the peak pressure conditions, and restrict our discussion to contributions that use up to date thermodynamic data sets and incorporate the effects of bulk rock composition including, where appropriate, the effect of fractionation of elements during mineral growth (Figs. 4 and 5A). These *P–T* paths all show steep *P*/*T* slopes and do not project back to the origin (Fig. 5A); subduction *P–T* paths necessarily start close to the origin so this implies an upward concave subduction *P–T* path (see also Aoya et al., 2003).

The rapid subduction of the Izanagi plate of vs = 20–24 cm/yr means that *P–T* conditions along the slab surface approach steady state a few million years after subduction initiation (Figs. 5A, B). In addition, the association of the rapid subduction with a high μ' value results in the development of steep inverted temperature gradients within the slab close to the subduction boundary. For example, using values of vs = 24 cm/yr and μ' = 0.13, in the range 0.6–2 GPa there is a reduction in temperature of ~100 ºC to ~80 ºC moving 1 km downwards away from the slab surface (Fig. 5A). These large temperature differences result from the high frictional heating along the subduction boundary that peaks at a depth of ~ 20 km (Fig. 5F) and strong advective cooling of subduction (Fig. 5C). If μ' is reduced to 0.06, the temperature gradient within the slab close to the subduction boundary decreases with the temperature difference at a pressure of 0.6 GPa reducing from ~100°C to ~80 ºC (Fig. 5B). This reflects a lower frictional heating that peaks at a depth of ~ 35 km (Fig. 5F).

A series of calculations show that while both μ' (frictional stresses) and *f* (viscous stresses) affect *P–T* conditions along the subduction boundary, the *P*/*T* slope at *P* = 1–2 GPa is largely controlled by μ' (Fig. 5E). This relationship reflects the greater depth of the peak of shear stress, and hence shear heating, for lower μ' (Fig. 5F). We also examined the effect of subduction rate and direction (Fig. 5G–I). For the same μ' and *f*, a slower subduction rate results in a lower temperature along the slab surface and a smaller difference in temperature between the slab surface and a surface 1 km deeper within the slab (Fig. 5G). Steeper *P–T* paths are predicted for lower values of *f*, which decreases shear heating in the deeper ductile region and/or larger values of μ', which increases shear heating in the shallower frictional region (Fig. 5H). Varying the obliquity of convergence has only a small effect: trench-normal subduction (ϕ = 0º) results in a slightly lower temperature along the subduction boundary compared with oblique subduction (ϕ = 30º) due to the greater advective cooling (Fig. 5I).

A comparison between the observed *P–T* paths and the results of the calculations shows that significant amounts of shear heating are required to account for the observed steep gradients and curvature of the subduction-related Sanbagawa *P–T* paths (Fig. 5A, E). The two warmest paths are well matched by conditions close to the subduction boundary for μ'~ 0.13 and *f* ~ 1. These paths are recorded in central Shikoku and eastern Kii peninsula where kilometer-scale remnants of the mantle wedge are also preserved (e.g. Endo et al., 2013; Wallis & Aoya, 2000) suggesting that they were derived from close to the subduction boundary. The other *P–T* paths are compatible with μ' ~ 0.13 if a domain up to 1 km perpendicular distance from the subduction boundary is considered—a distance that is reasonable considering the geometry of eclogite units in the Sanbagawa belt (Wallis and

Aoya, 2000; Kouketsu et al., 2014). However, taken in isolation these *P*–*T* paths could also be accounted for with lower values of $\mu' \geq 0.06$ (Fig. 5E). For lower subduction rates, the warm conditions can be accounted for by some combination of lager values of viscous shear, *f*, and larger values of μ' (Fig. 5H). However, a larger value of μ' is required to cover the full range of *P*–*T* paths, including the steeper parts, because an increase in *f* results in warmer conditions in the deeper part of the subduction boundary and a concomitant decrease in *P*/*T* slope (Fig. 5H).

From the above considerations, we propose two possible models for the stress state of the Sanbagawa subduction boundary at ~90Ma. (i) There was relatively high stress throughout the region with $\mu' \geq 0.13$ and peak shear stresses up to about 60 MPa (Fig. 5F). In this case, differences in *P*–*T* paths reflect variable distances from the subduction boundary and only the highest temperature *P*–*T* paths reflect conditions close the subduction boundary (Fig. 5A). (ii) Stress was variable and differences in the *P*–*T* paths reflect along-strike spatial differences in μ' ranging from a minimum of 0.06 in the east of Shikoku, bordered to the east and west by stronger domains with $\mu' \geq 0.13$ (Fig. 5E).

4.2. Franciscan Belt

The Franciscan belt, western USA (Fig. 6), is an accretionary complex reflecting the history of a long-lived (ca. 170–25 Ma) convergent plate boundary (Wakabayashi, 2015). The highest grade metamorphic rocks generally occur as mafic blocks, and more rarely coherent sheets, metamorphosed in the eclogite and blueschist facies. Although there is evidence for sedimentary reworking of many of the blocks, they commonly display metasomatic rinds showing they were originally surrounded by serpentinite. These high-grade blocks constitute the oldest part of the metamorphic sequence (>150 Ma) (Anczkiewicz et al., 2004; Cooper et al., 2011; Mulcahy et al., 2014) and record conditions shortly after the initiation of subduction. The rinds developed during retrograde metamorphism and show similar but slightly younger ages around 150 Ma (Wakabayashi, 2015 and references therein). These results indicate early exhumation of the high-grade blocks within a serpentinite-dominated mélange (Wakabayashi, 2015 and references therein). The mafic units are generally a few meters to tens of meters thick and their prograde *P–T* conditions should closely reflect conditions in a thin layer along the former subduction boundary.

Subduction of the Franciscan metamorphic rocks under the Coast Range Ophiolite (CRO) started at around 165–170 Ma (Wakabayashi, 2015). The overlap in age between the high-grade Franciscan metamorphism (ca. 150–169 Ma) and the igneous formation of the CRO (165–172 Ma) implies subduction initiated immediately after the formation of the CRO (Wakabayashi, 2015, and references therein). In addition, the high-grade rocks have an arc-like geochemical signature typical of a supra-subduction origin. Taken together these results imply subduction initiated at or close to a spreading ridge (Wakabayashi, 2015 and references therein), and in our modelling we use a young (10 Ma) oceanic overriding plate and a subducting plate age of 10 Ma. After subduction begins, the inflow of cool oceanic lithosphere causes cooling until steady state is achieved. Metamorphic rocks subducted during this period of cooling will rise back to the surface following a cooler *P–T* path than when they were subducted. The well-documented anti-clockwise *P-T* paths of the high-grade blocks of the Franciscan belt (Krogh et al., 1994; Page et al, 2007; Tsujimori et al., 2006a) are good supporting evidence that they were indeed subducted during the initial cooling phase shortly after the onset of subduction. Differences in radiometric ages suggest that most of the cooling in the Franciscan subduction zone took place over a period of 10–20 million years (Fig. 7A). We consider this time scale in our modelling, which includes a close examination of the early thermal evolution of the modelled subduction zone before steady state was achieved.

Numerous studies have been carried out to determine peak *P–T* conditions and *P–T* paths of the high-grade Franciscan blocks (e.g. Krogh et al., 1994; Page et al, 2007; Tsujimori et al., 2006a). A major point of disagreement arises from different calibrations for the garnet–phengite–clinopyroxene thermobarometer. The Ravna and Terry calibration (Ravna and Terry 2004) yields higher pressures than the Waters–Martin calibration (Wain et al. 2001). Hereafter, we refer to these as the RT and WM calibrations, respectively and compare our model results with both sets of *P–T* estimations.

For relatively fast subduction of vs = 10 cm/yr, most *P–T* conditions and their associated ages are well explained by assuming $\mu' = 0$ irrespective of calibration methods (Fig. 7A). Increasing μ' even a small amount increases the temperature of the subduction boundary to values significantly greater than the estimated *P–T* conditions; appropriate upper bounds are $\mu' = 0.02$ (RT) and 0.03 (WM) (Fig. 7B). An increase in the subduction rate leads to greater frictional heating but also increases the cooling effect by advection of cold lithosphere and has only a small effect on the model results (Fig. 7C). Lower subduction rates can also be considered, but this causes an increase in the expected temperature; approximate lower bounds for zero frictional heating are vs = 6 cm/yr (RT) and 4 cm/yr (WM) (Fig. 7D). Increasing the age of the subducting plate to 30 Ma yields results that suggest $\mu' < 0.03$ and vs > 4 cm/yr (RT) and $\mu' < 0.05$ and vs > 2 cm/yr (WM) (Fig. 8). The above analysis shows the *P–T* conditions recorded by the Franciscan high-grade blocks constrain the shear heating to be very low with an appropriate upper bound of $\mu' = 0.03$.

5. Discussion

5.1. Factors controlling stress state along subduction boundaries

Our results for the Sanbagawa and Franciscan belts show where there is suitable information available on aspects of ancient subduction systems such as subduction rate, slab age and elapsed time after subduction initiation, the subduction-related *P–T* paths and peak P–T conditions of metamorphic rocks can be used to place bounds on the frictional heating and, hence, shear stresses acting along ancient subduction boundaries. The value of μ'~ 0.13 estimated for the Sanbagawa belt and the upper bound of μ'~ 0.03 estimated for the Franciscan belt are in good agreement with the range of estimates of μ' for currently active subduction zones (see Fig. 1). In this section, we discuss factors controlling the stress state along subduction boundaries.

Laboratory experiments show that the coefficient of friction decreases from ~0.7 to ~0.1 as slip rates increase up to seismic rates of ~1 m/s; results that are essentially independent of rock type and weakening mechanism (Di Toro et al., 2011). These observations imply that subduction megathrusts are expected to move under low stress conditions during co-seismic slip at high slip rates and high stress during periods of creep at the plate convergence rate. The seismic coupling coefficient—defined as the ratio between the observed seismic moment release rate and the rate calculated from plate tectonic velocities (Scholz and Campos, 2012)—may, therefore, help shed light on variations of shear stresses in active subduction zones. One example is the northern Hikurangi subduction boundary, which has a seismic coupling coefficient of ~0 (Scholz and Campos, 2012) implying creep-dominant slip. Gao and Wang (2014) estimate a relatively high μ' of ~0.13 for this region. In addition, high seismic coupling coefficients of 0.5–1 are associated with subduction boundaries in Central Chile, Cascadia, Kamchatka, Honshu, Nankai, and Sumatra where estimates of μ' are low (0.02–0.03). The high μ' value and aseismic creep of the northern Hikurangi subduction boundary may be controlled by the rugged surface topography of the subducting oceanic plate

(Wang and Bilek, 2014; Gao and Wang, 2014). In this study we assume a constant μ' along the subduction megathrust, implying a temporal and spatial average. We note that this average is with respect to slip distance, because the shear stress during the no-slip period does not contribute to shear heating.

Another factor controlling the shear stress along subduction boundary may be subduction rate. Slip behaviour along the subduction megathrust changes from shallow co-seismic slip to deep stable slip with a domain of slow slip in between. The down-dip seismogenic limit and the transition from velocity-weakening to velocity-strengthening frictional behaviour along subduction megathrusts is considered to be temperature-dependent (Hyndman et al., 1997; Den Hartog and Spiers, 2013), and a shallower down-dip seismogenic limit is expected for a higher temperature subduction boundary. Therefore, the depth range of aseismic, semi-frictional slip associated with a relatively high degrees of shear heating is expected to be wider for a higher temperature subduction boundary. This positive feedback process, where higher temperature subduction boundaries overall generate greater frictional heat than lower temperature boundaries, combined with the tendency for velocity-strengthening aseismic creep to dominate under extremely high subduction rates (vs > 20 cm/yr), may be the cause of the high shear stresses and high temperature of the Sanbagawa subduction boundary.

Deformation in the deeper parts of subduction boundaries will be controlled by a viscous rheology. In contrast to frictional behaviour, differences in viscous rheology mainly depend on rock type. Experimentally determined flow laws show that the viscosity of relevant rocks and constituent minerals (olivine, antigorite, basalt, eclogite, quartz and biotite) varies by more than five orders of magnitude (Agard et al., 2016 and references therein). In the subduction boundary zone antigorite serpentinite is likely to be one of the weakest major components followed by metasediment, metabasite and peridotite in order of increasing viscosity under conditions appropriate for the deeper part of subduction megathrust (400–700 ºC and strain rates of 10^{-12}–10^{-13}/s). While high-grade rocks in the Franciscan exhumed as blocks in serpentinite matrix (Wakabayashi, 2015), the eclogite unit of the Sanbagawa belt consists of continuous mafic and pelitic schist layers including ultramafic blocks (Wallis and Aoya, 2000; Kouketsu et al., 2014). Therefore, in addition to subduction velocity, the contrasting difference in shear stress between these two ancient subduction boundaries may reflect the difference in deformation accommodating rock types of the high-grade units.

5.2. Additional factors relevant to the estimation of μ'

5.2.1. Fluid flow and advective heat transport

Recent studies have shown that hydrothermal circulation in the basement aquifer of subducting oceanic crust has a large effect on the temperature along subduction boundaries (Spinelli et al., 2018 and references therein). This hydrothermal circulation mines heat from subducted crust and transports it seaward, resulting in higher temperatures in areas seaward of the trench and lower temperatures in the subduction zone, when compared to temperatures expected in the absence of the hydrothermal circulation. Numerical modelling shows that hydrothermal circulation can reduce temperatures along subduction boundaries by up to ~100 ºC and is especially large for hot subduction zones, such as the Cascadia and Nankai subduction zones (Spinelli et al., 2018 and references therein). Although many difficulties exist in estimating the effect of hydrothermal circulation, such as the evolution of permeability with depth, its relation with subduction parameters and the areal extent of any circulation cell, incorporating the effects of such fluid circulation in our discussion would require higher values of μ' and would be particularly large for the relatively hot Sanbagawa subduction. We also note that the exhumation of metamorphic rocks also involves advective heat transport from depth to surface and incorporating such effects in thermo-mechanical models of subduction would represent a significant increase in complexity. For our purposes it is more appropriate to focus on well-constrained prograde subduction-related *P–T* paths that are unaffected by this complication.

5.2.2. Slab geometry

There are no good constraints on the original dip of the subduction boundary for ancient subduction zones, and we use a typical geometry for active subduction zones: slab surface dip gradually increases up to 30º at 30 km depth, that is ~150 km horizontal distance from trench (Fig. 2). An increase in the subduction angle results in a lower temperature along the subduction boundary through two processes: (1) an increase in advective cooling due to increase in downward velocity of subducting plate and (2) a decrease in the fault length over which frictional processes operate and hence a decrease in shear heating. To examine this effect more closely, we conducted calculations for different geometrical configurations including shorter boundary lengths for the depth range of < 30 km, and thus higher average slab dips. For the Sanbagawa subduction, the result shows a lower temperature and slightly shallower P/T slope along subduction boundary (Fig. 9). For these conditions, a larger value of μ' is required to account for the *P–T* paths. For the Franciscan subduction, the range of required conditions shifts slightly towards higher μ' and *vs*.

5.3. Comparison with previous models

To examine the consistency of our model results with those of previous studies, in Fig. 3A we show the results for similar subduction parameters presented by van Keken et al. (2018) in a study of active subduction. Our model shows a close correspondence with these results if zero frictional heating is assumed (Fig. 3A). An important point raised in several previous studies is that for pressures of 1–2 GPa the prograde *P–T* conditions for exhumed subduction-related metamorphic rocks on average show temperatures 100–350 ºC higher than the average modelled *P–T* conditions for active subduction boundaries (e.g. Aoya et al. 2003; Penniston-Dorland et al., 2015). To account for this discrepancy some workers have suggested that weaker warm rocks are more likely to reach the earth's surface by buoyant flow and the rock record is biased (van Keken et al., 2018). However, others suggest that the discrepancy may be due to a greater component of frictional heating than is commonly included in thermal models (Penniston-Dorland et al., 2015; Kohn et al., 2018). The conditions (*age* and *vs*) shown in Fig. 3 covers a range appropriate for almost all active subduction margins including NE Japan and Cascadia—good representatives of cold and hot margins, respectively—and we can use these results to discuss global trends. Red lines in Fig. 3A show the range of prograde *P–T* conditions for exhumed subduction-related metamorphic rocks (Figure 2b of van Keken et al., 2018). Our modelling shows the *P–T* profiles for cold subduction zones with typical values of *age* = 100 Ma and *vs* = 10 cm/yr are broadly compatible with the coolest rock records provided that $\mu' \geq 0.02$. This result is consistent with previous estimates for the strength of many active subduction boundaries (Fig. 1). In contrast, the higher temperature rock records (>500°C, $\leq$2 GPa) are only achieved in (i) slow subduction of very young slabs, (ii) the conditions shortly after the initiation of subduction, or (iii) associated with high amounts of shear heating. The highest temperature rock records (>700 ºC, $\leq$2 GPa) most likely represent the conditions shortly after the initiation of subduction (e.g. *P–T* profile for *t* = 5 Myr in Fig. 7) but could also be accounted for by very high amounts of viscous shear heating (Fig. 5E). As we show here, with sufficient geological constraints on ancient subduction conditions, it is possible to distinguish between these situations using the rock record. For situations where μ’ ≥ 0.03, shear heating has significant components from viscous shear as well as frictional shear (Figs. 3B, 5F).

6. Conclusions

Thermal modelling of subduction zones that incorporates frictional and viscous shear heating shows significant differences in temperature that have the potential of being recorded in the rock record. Where information is available on past plate subduction rate, slab age and time since the onset of subduction, the *P–T* history of subduction-type metamorphism can be used to place bounds on the shear stresses and strength of subduction zones. The overall strength and the associated shear stresses can be expressed by the effective coefficient of friction, μ’, applicable to the friction-dominant shallow part of the subduction boundary. The Sanbagawa belt of SW Japan was formed by rapid subduction of a 60 Ma slab. Relatively high-stresses (μ’ ≥ 0.13) can be identified by the presence of strongly curved *P–T* paths that increase in *P/T* gradient up to a pressure of about 2 GPa. The rate of subduction of the Franciscan belt, W. USA is less well constrained, but the cool prograde *P–T* paths constrain shear heating, and hence shear stresses, to be very limited with an appropriate upper bound for μ’ of ~0.03. The range of μ’ estimated in this study shows good agreement with independent estimates for modern subduction zones. Our modelling shows the rate of subduction and lithological makeup of the subduction boundary zone are important factors in determining the stress on subduction boundaries. High stress subduction zones are likely to be associated with high aseismic/seismic slip ratios possibly related to slab roughness.

Acknowledgements

We thank S. Endo and T. Tsujimori for helpful discussions during the preparation of this manuscript. We also thank An Yin for his editorial handling as well as an anonymous reviewer for his/her constructive comments that helped improve the manuscript. SW acknowledges support for this research from the JSPS grant in aid 16H06476.

Appendix A. Numerical method

Conservation of mass is approximated by the incompressible continuity equation,

$$\frac{\partial v_x}{\partial x} + \frac{\partial v_z}{\partial z} = 0 \tag{A1}$$

where v_x and v_z are the horizontal and vertical components of the velocity vector, respectively. The two-dimensional Stokes equations for creeping flow take the form

$$\frac{\partial \sigma_{xx}}{\partial x} + \frac{\partial \sigma_{xz}}{\partial z} = \frac{\partial P}{\partial x} \tag{A2}$$

$$\frac{\partial \sigma_{zz}}{\partial z} + \frac{\partial \sigma_{xz}}{\partial x} = \frac{\partial P}{\partial z} - \rho g \tag{A3}$$

where σ_{xx}, σ_{zz}, and σ_{xz} are the components of the deviatoric stress tensor, P is pressure, g is acceleration due to gravity, density ρ is given by the expression

$$\rho = \rho_0\big(1 - \alpha(T - T_0)\big)\big(1 + \beta(P - P_0)\big) \tag{A4}$$

where ρ_0 is the standard density at P_0 = 0.1 MPa and T_0 = 273 K, and $\alpha = 3.1 \times 10^{-5}$ /K and $\beta = 1.0 \times 10^{-11}$ /Pa (Turcotte and Schubert, 2002) are the thermal expansion and compressibility coefficients, respectively. The standard density values ρ_0 for the mantle, oceanic crust, continental lower crust, and continental upper crust are 3300, 3000, 3000, and 2700 kg/m^3, respectively (Turcotte and Schubert, 2002).

To calculate the flow field in the mantle wedge, we use an experimentally determined constitutive flow law for the dislocation creep of olivine aggregates (Karato and Wu, 1993),

$$\dot{\varepsilon} = A\, \sigma^n exp\left(-\frac{Ea + VaP}{RT}\right) \tag{A5}$$

where $\dot{\varepsilon}$ is the strain rate, $A = 2.42 \times 10^5$ /(MPa^n s) is the pre-exponential factor, σ is stress, n = 3.5 is the stress exponent, Ea = 540 kJ/mol is activation energy, and $Va = 15 \times 10^{-6}$ m^3/mol is activation volume, R is the universal gas constant, T is absolute temperature, and P is pressure.

The energy equation takes the form

$$\rho C_p \left(\frac{\mathrm{D}T}{\mathrm{D}t}\right) = \frac{\partial q_x}{\partial x} + \frac{\partial q_z}{\partial z} + H_r + H_a + H_f + H_s$$

$$q_x = \kappa \frac{\partial T}{\partial x}, \quad q_z = \kappa \frac{\partial T}{\partial z} \qquad \text{(A6)}$$

$$H_a \approx T\alpha\rho v_z g \,, \qquad H_s \approx \sigma_{xx}\sigma\dot{\varepsilon}_{xx} + \sigma_{zz}\sigma\dot{\varepsilon}_{zz} + \sigma_{xz}\sigma\dot{\varepsilon}_{xx}$$

where q_x and q_z are horizontal and vertical heat fluxes, and $\dot{\varepsilon}_{xx}$, $\dot{\varepsilon}_{zz}$, and $\dot{\varepsilon}_{xz}$ are components of the strain rate tensor. The thermal conductivities κ of the crust and mantle are 2.5 and 3.1 W/m K, respectively (Peacock and Wang, 1999). The terms H_r, H_a, H_f, and H_s, denote heat productions in W/m^3. H_a is the adiabatic heating and H_s is viscous shear heating within the mantle wedge. The radioactive heat production values H_r for the mantle, oceanic crust, continental lower crust, and continental upper crust are 0, 0.27, 0.27, and 1.3 μW/m^3, respectively (Peacock and Wang, 1999). Shear heating H_f, calculated from Equations (1)–(4) in the main text, is imposed along subduction interface from trench to the depth of Dc + 10 km. The isobaric heat capacity C_P is assumed to be 1200 J/kg K.

References

Agard, P., Yamato, P., Soret, M., Prigent, C., Guillot, S., Plunder, A., Dubacq, B., Chauvet, A., Monié, P., 2016. Plate interface rheological switches during subduction infancy: Control on slab penetration and metamorphic sole formation. Earth Planet. Sci. Lett. 451, 208–220. https://doi.org/10.1016/j.epsl.2016.06.054.

Anczkiewicz, R., Platt, J.P., Thirlwall, M.F., Wakabayashi, J., 2004. Franciscan subduction off to a slow start: evidence from high-precision Lu–Hf garnet ages on high grade-blocks. Earth Planet. Sci. Lett. 225, 147–161. doi: 10.1016/j.epsl.2004.06.003.

Aoki, S., Aoki, K., Tsuchiya Y., Kato, D., 2019. Constraint on the eclogite age of the Sanbagawa metamorphic rocks in central Shikoku, Japan. Int. Geol. Rev. 61, 2211-2226. https://doi.org/10.1080/00206814.2019.1581997

Aoya, M., Uehara, S., Matsumoto, M., Wallis, S.R., Enami, M., 2003. Subduction-stage pressure–temperature path of eclogite from the Sambagawa belt: prophetic record for oceanic-ridge subduction. Geology 31, 1045–1048. https://doi.org/10.1130/G19927.1.

Cooper, F.J., Platt, J.P., Anczkiewicz, R., 2011. Constraints on early Franciscan subduction rates from 2-D thermal modeling. Earth Planet. Sci. Lett. 312, 69–79. https://doi.org/10.1016/j.epsl.2011.09.051.

den Hartog, S.A.M., Spiers, C.J., 2013. Influence of subduction zone conditions and gouge composition on frictional slip stability of megathrust faults. Tectonophysics 600, 75–90. https://doi.org/10.1016/j.tecto.2012.11.006.

Di Toro G, Han R, Hirose T, De Paola N, Nielsen S, Mizoguchi K, Ferri F, Cocco M, Shimamoto T, 2011. Fault lubrication during earthquakes: Nature 471, 494–498. https://doi.org/10.1038/nature09838.

Endo, S., Wallis, S.R., Hirata, T., Anczkiewicz, R., Platt, J., Thirlwall, M., Asahara,Y., 2009. Age and early metamorphic history of the Sanbagawa belt: Lu–Hf and *P–T* constraints from the Western Iratsu eclogite. J. Metamorph. Geol. 27, 371–384. https://doi.org/10.1111/j.1525-1314.2009.00821.x.

Endo, S., Nowak, I. Wallis, S. R., 2013. High-pressure garnet amphibolite from the Funaokayama unit, western Kii Peninsula and the extent of eclogite facies metamorphism in the Sanbagawa belt. J. Mineral. Petrol. Sci. 108, 189–200.

Engebretson, D.C., Cox, A., Gordon, R.G., 1985. Relative motion between oceanic and continental plates in the Pacific basin. Geol. Soc. Am. Spec. Paper 206, 59 p.

England, P., 2018. On shear stresses, temperatures, and the maximum magnitudes of earthquakes at convergent plate boundaries. J. Geophys. Res. 123, 7165–7202. https://doi.org/10.1029/2018JB015907.

Evans, B., Kohlstedt, D.L., 1995. Rheology of rocks. in: Ahrens, T.J. (Ed.), Rock physics and phase relations—A handbook of physical constants. Am. Geophys. Union Reference Shelf 3, pp. 148–165.

Gao, X., and Wang, K., 2014. Strength of stick-slip and creeping subduction megathrusts from heat flow observations: Science 345, 1038–1041. https://doi.org/10.1126/science.1255487.

Gerya, T.V., and Yuen, D.A., 2003. Characteristics-based marker-in-cell method with conservative finite-differences schemes for modeling geological flows with strongly variable transport properties. Phys. Earth Planet. Inter. 140, 293–318.

Hyndman, R.D., Yamano, M., Oleskevich, D.A., 1997. The seismogenic zone of subduction thrust faults. Island Arc 6, 244–260.

Kabir, M.F., and Takasu, A., 2016. Jadeite–garnet glaucophane schists in the Bizan area, Sambagawa metamorphic belt, eastern Shikoku, Japan: significance and extent of eclogite facies metamorphism. J. Metamorph. Geol. 34, 893–916. https://doi.org/10.1111/jmg.12198.

Karato, S., Wu, P., 1993. Rheology of the upper mantle: A synthesis. Science 260, 771–778. https://doi.org/10.1126/science.260.5109.771.

Knittel, U., Suzuki, S., Nishizaka, N., Kimura, K., Tsai, W.-L., Lu, H.-Y., Ishikawa, Y., Ohno, Y., Yanagida, M., Lee, Y.-H., 2014. U–Pb ages of detrital zircons from the Sanbagawa Belt in western Shikoku: Additional evidence for the prevalence of Late Cretaceous protoliths of the Sanbagawa Metamorphics. J. Asian Earth Sci. 96, 148–161. https://doi.org/10.1016/j.jseaes.2014.09.001

Kohn, M.J., Castro, A.E., Kerswell, B.C., Ranero, C.R., Spear, F.S., 2018. Shear heating reconciles thermal models with the metamorphic rock record of subduction: Proc. National Acad. Sci. 115, 11706-11711. https://doi.org/10.1073/pnas.1809962115.

Kouketsu, Y., Enami, M., Mouri, T., Okamura, M., Sakurai, T., 2014. Composite metamorphic history recorded in garnet porphyroblasts of Sanbagawa metasediments in the Besshi region, central Shikoku, Japan. Island Arc 23, 263–280. https://doi.org/10.1111/iar.12075.

Krogh, E.J., Oh, C.W., Liou, J.G., 1994. Polyphase and anticlockwise *P–T* evolution for Franciscan eclogites and blueschists from Jenner, California, USA. J. Metamorph. Geol. 12, 121–134. https://doi.org/10.1111/j.1525-1314.1994.tb00008.x.

Lamb, S., 2006. Shear stresses on megathrusts: Implications for mountain building behind subduction zones. J. Geophys. Res. 111, B07401. doi: 10.1029/2005JB003916.

Luan, F.C., Paterson, M.S., 1992. Preparation and deformation of synthetic aggregate of quartz. J. Geophys. Res. 97, 301–320. https://doi.org/10.1029/91JB01748.

Maruyama, S., Isozaki, Y., Kimura, G., Terabayashi, M., 1997. Paleogeographic maps of the Japanese Islands: Plate tectonic synthesis from 750 Ma to the present. Island Arc 6, 121-142. https://doi.org/10.1111/j.1440-1738.1997.tb00043.x

Mulcahy, S., Vervoort, J.D., Renne, P.R., 2014. Dating subduction zone metamorphism with combined garnet and lawsonite Lu-Hf geochronology: J. Metamorph. Geol. 32, 515–533. https://doi.org/10.1111/jmg.12092.

Müller, R.D., Seton, M., Zahirovic, S., Williams, S.E., Matthews, K.J., Wright, N.M., Shephard, G.E., Maloney, K.T., Barnett-Moore, N., Hosseinpour, M., Bower, D.J., Cannon, J., 2016. Ocean basin evolution and global-scale plate reorganization events since Pangea breakup. Ann. Rev. Earth Planet. Sci. 44, 107–138. https://doi.org/10.1146/annurev-earth-060115-012211.

Noda H., Shimamoto, T., 2012. Transient behavior and stability analyses of halite shear zones with an empirical rate-and-state friction to flow law. J. Struct.l Geol. 38, 234-242. https://doi.org/10.1016/j.jsg.2011.08.012.

Nozaki, T., Kato, Y., Suzuki, K., 2013. Late Jurassic ocean anoxic event: evidence from voluminous sulphide deposition and preservation in the Panthalassa. Sci. Rep. 3, 1889. https://doi.org/10.1038/srep01889.

Okamoto, K., Shinjoe, H., Katayama, I., Terada, K., Sano Y., Johnson, S., 2004. SHRIMP U–Pb zircon dating of quartz-bearing eclogite from the Sanbagawa Belt, south-west Japan: implications for metamorphic evolution of subducted protolith. Terra Nova 16, 81–89. https://doi.org/10.1111/j.1365-3121.2004.00531.x.

Osei Tutu, A., Sobolev, S.V., Steinberger, B., Popov, A.A., Rogozhina, I., 2018. Evaluating the influence of plate boundary friction and mantle viscosity on plate velocities. Geochem. Geophys. Geosyst. 19, 642–666. https://doi.org/10.1002/2017GC007112.

Page, F.Z., Armstrong, L.S., Essene E.J., Mukasa S.B., 2007. Prograde and retrograde history of the Junction School eclogite, California, and an evaluation of garnet–phengite–clinopyroxene thermobarometry. Contr. Mineral. Petrol. 153, 533–555. https://doi.org/10.1007/s00410-006-0161-9.

Peacock, S.M., 1992. Blueschist facies metamorphism, shear heating, and *P–T–t* paths in subduction shear zones. J. Geophys. Res. 97, 17693–17707.

Peacock, S.M., Wang, K., 1999. Seismic consequences of warm versus cool subduction metamorphism: examples from southwest and northeast Japan. Science 286, 937-939. https://doi.org/10.1126/science.286.5441.937.

Penniston-Dorland, S.C., Kohn, M.J., Manning, C.E., 2015. The global range of subduction zone thermal structures from exhumed blueschists and eclogites: Rocks are hotter than models. Earth Planet. Sci. Lett. 428, 243–254. https://doi.org/10.1016/j.epsl.2015.07.031

Ravna E.J.K., Terry M.P., 2004. Geothermobarometry of UHP and HP eclogites and schists—an evaluation of equilibria among garnet–clinopyroxene–kyanite–phengite–coesite/quartz. J. Metamorph. Geol. 22, 579–592.

Scholz, C. H., J. Campos, 2012. The seismic coupling of subduction zones revisited. J. Geophys. Res., 117, B05310. https://doi.org/10.1029/2011JB009003.

Spinelli, G., Wada, I., Wang, K., He, J., Harris, R., Underwood, M., 2018. Diagenetic, metamorphic, and hydrogeologic consequences of hydrothermal circulation in subducting crust. Geosphere 14, 2337–2354. https://doi.org/10.1130/GES01653.1.

Stein, C.A., Stein, S., 1992. A model for the global variation in oceanic depth and heat flow with lithospheric age. Nature 359, 123–129. https://doi.org/10.1038/359123a0.

Tsujimori, T., Matsumoto, K., Wakabayashi, J., Liou, J.G., 2006a. Franciscan eclogite revisited: Reevaluation of the *P–T* evolution of tectonic blocks from Tiburon Peninsula, California, U.S.A. Mineral. Petrol. 88, 243–267. https://doi.org/10.1007/s00710-006-0157-1.

Tsujimori, T., Sisson, V.B., Liou, J.G., Harlow, G.E., Sorensen, S.S., 2006b. Very-low-temperature record of the subduction process: A review of worldwide lawsonite eclogites. Lithos 92, 609–624. https://doi.org/10.1016/j.lithos.2006.03.054.

Turcotte, D.L., Schubert, G., 2002. Geodynamics, second ed. Cambridge Univ. Press, Cambridge.

van Keken, P.E., Wada, I., Abers, G.A., Hacker, B.R., Wang, K., 2018. Mafic high-pressure rocks are preferentially exhumed from warm subduction settings. Geochem. Geophys. Geosyst. 19. https://doi.org/10.1029/2018GC007624.

Wada, I., Wang, K., 2009. Common depth of slab-mantle decoupling: reconciling diversity and uniformity of subduction zones: Geochem. Geophys. Geosyst. 10, Q10009. https://doi.org/10.1029/2009GC002570.

Wain AL, Waters DJ, Austrheim H, 2001. Metastability of granulites and processes of eclogitisation in the UHP region of western Norway. J. Metamorph. Geol. 19, 607–623.

Wakabayashi, J., 2015. Anatomy of a subduction complex: architecture of the Franciscan Complex, California, at multiple length and time scales. Int. Geol. Rev. 57, 669–746. https://doi.org/10.1080/00206814.2014.998728.

Wallis, S.R., Anczkiewicz, R., Endo, S., Aoya, M., Platt, J.P., Thirlwall, M. Hirata, T., 2009. Plate movements, ductile deformation and geochronology of the Sanbagawa belt, SW Japan: tectonic significance of 89–88 Ma Lu–Hf eclogite ages. J. Metamorph. Geol. 27, 93–105. https://doi.org/10.1111/j.1525-1314.2008.00806.x.

Wallis, S.R. Aoya, M., 2000.A re-evaluation of eclogite facies metamorphism in SW Japan: proposal for an eclogite nappe. J. Metamorph. Geol. 18, 653–664.

Wallis, S.R. Okudaira, T., 2016. Paired metamorphic belts of SW Japan: the geology of the Sanbagawa and Ryoke metamorphic belts and the Median Tectonic Line. in: Moreno, T., Wallis, S.R., Kojima, T., Gibbon W. (Eds.), The Geology of Japan. Geol. Soc. London. pp. 101–124.

Wang, K., and Bilek, S.L., 2014, Fault creep caused by subduction of rough seafloor relief. Tectonophysics 610, 1–24. https://doi.org/10.1016/j.tecto.2013.11.024.

Weller, O.M., Wallis, S. R., Aoya, M., Nagaya, T., 2015. Phase equilibria modelling of blueschist and eclogite from the Sanbagawa metamorphic belt of southwest Japan reveals along-strike consistency in tectonothermal architecture: J. Metamorph. Geol. 33, 579–596. https://doi.org/10.1111/jmg.12134.

FIGURE CAPTIONS

Fig. 1. Apparent coefficient of friction along active subduction boundaries estimated from heat flow (red, Gao & Wang (2014); green, England (2018)) and force balance (blue, Lamb (2006)). Black lines show apparent coefficient of friction along ancient subduction boundaries estimated in this study.

Fig. 2. (A) Model geometry and boundary conditions. The boundary conditions for flow in mantle the wedge are shown in blue, and those for temperature are shown in red. (B) Initial temperature distribution for a case with an overriding continental plate.

Fig. 3. (A) Temperature distribution along the slab surface as a function of subducting plate age (*age* = 10, 30, 100 Ma), subduction rate (*vs* = 3, 10 cm/yr), and apparent coefficient of friction (μ' = 0, 0.01, 0.03, 0.1, 0.2) with an overriding continental plate, *Dc* = 80 km, *f* = 1, and elapsed time *t* = 30 Myr. Green lines show slab surface conditions for current subduction margins (Central Honshu, Nicaragua, Cascadia) at 30 Myr after subduction initiation as calculated by van Keken et al. (2018). Red lines show the range (2σ) of prograde metamorphic *P-T* conditions (van Keken et al., 2018). (B) Shear stress along the decoupled section of the subduction boundary for the same conditions as A. (C) Temperature distributions for *age* = 100 Ma, *vs* = 3 cm/yr, and μ' = 0, 0.1. For μ' = 0.1, the high *T* zone along the subduction boundary is the result of high frictional heating. Black arrows show the velocity field in the mantle wedge.

Fig. 4. Distribution of the Sanbagawa belt in SW Japan. Analyses of samples from the four areas shown by stars were used to derive the *P-T* paths shown in Fig. 5A.

Fig. 5. (A) Subduction *P–T* paths of the Sanbagawa metamorphic belt compared with model results. *age* = 60 Ma, *vs* = 24 cm/yr, *Dc* = 70 km, $\phi = 30^{\circ}$, $\mu' = 0.13$, *f* = 1 and with an overriding continental plate. Black lines show temperatures along the slab surface at *t* = 0, 1, 2, 5, 30 Myr and the gray line shows the temperature 1 km below the slab surface at *t* = 30 Myr. 1 = Endo et al. (2009), 2 and 3 = Weller et al. (2015), 4 = Kabir and Takasu (2016), 5 = Endo et al. (2013). (B) Same as A except $\mu' = 0.06$. (C) Temperature distribution for the same conditions as A at *t* = 30 Myr. (D) Temperature distribution for the same conditions as B at *t* = 30 Myr. (E) Slab surface conditions as a function of μ' (0, 0.03, 0.06, 0.13, 0.2) and *f* (0.5, 1, 2). *vs* = 24 cm/yr, *t* = 30 Myr, *age* = 60 Ma, *Dc* = 70 km, $\phi = 30^{\circ}$ and an overriding continental plate. (F) Shear stress along the decoupled section of the subduction boundary for the same conditions as E. (G) Effects of changing subduction velocity: i) the temperature along the slab surface is lower for a slower subduction rate; and ii) the temperature difference between the slab surface and 1 km below the slab surface is lower for a slower subduction rate. *vs* = 10, 24 cm/yr, $\mu' = 0.13$, *t* = 30 Myr, *age* = 60 Ma, *Dc* = 70 km, *f* = 1 and an overriding continental plate. (H) Slab surface *P–T* conditions as a function of *vs* (10, 24 cm/yr), μ' (0.06, 0.13) and *f* (0.5, 1, 2). *t* = 30 Myr, *age* = 60 Ma, *Dc* = 70 km, $\phi = 30^{\circ}$ and an overriding continental plate. (I) Effect of oblique subduction showing the temperature along the slab surface and 1 km below the slab surface is slightly lower for trench-normal subduction ($\phi = 0^{\circ}$) compared with oblique subduction ($\phi = 30^{\circ}$). *vs* = 24 cm/yr, *t* = 30 Myr, *age* = 60 Ma, *Dc* = 70 km, *f* = 1 and an overriding continental plate.

Fig. 6. Distribution of the Franciscan belt in USA. Stars show locations for samples that are used to derive the *P-T* conditions shown in Fig. 7A.

Fig. 7. Subduction *P–T* conditions of high-grade rocks in the Franciscan Complex compared with model results. Black lines show *P–T* conditions along the slab surface at t = 0, 2, 5, 10, 20 Myr. Values of *vs* and μ' are shown in each figure. *age* = 10 Ma, *Dc* = 80 km, ϕ = 0º, f = 1 and an overriding oceanic plate. *P-T* conditions: 1, 2 and 6 = Cooper et al. (2011), 3 = Krogh et al. (1994), 4 = Tsujimori et al. (2006a), 5 = Page et al. (2007), 7 = Tsujimori et al. (2006b). Metamorphic ages: 1, 2, 3 and 4 = Anczkiewicz et al. (2004), 6 = Cooper et al. (2011), 7 = Mulcahy et al. (2014).

Fig. 8. Subduction *P–T* conditions of high-grade rocks in the Franciscan Complex compared with model results. Black lines show *P–T* conditions along the slab surface at t = 0, 2, 5, 10, 20 Myr. Values of *vs* and μ' are shown in each figure. *age* = 30 Ma, *D*c = 80 km, ϕ = 0º, f = 1 and an overriding oceanic plate. *P-T* conditions and metamorphic ages are the same as in Fig. 7.

Fig. 9. Effect of slab geometry for the Sanbagawa subduction. *vs* = 24 cm/yr, μ' = 0.13, t = 30 Myr, *age* = 60 Ma, *Dc* = 70 km, ϕ = 30º, f = 1 and an overriding continental plate. (A) *P–T* profiles along the slab surface and 1 km below the slab surface. *P–T* paths are the same as in Fig. 5. (B) Slab geometry and temperature distribution for a steep slab dip. The length of the subduction boundary for depth range of < 30 km is shorter than that shown in Figs. 2B and 5C.

Ishii and Wallis, Figure 1
Single-column width

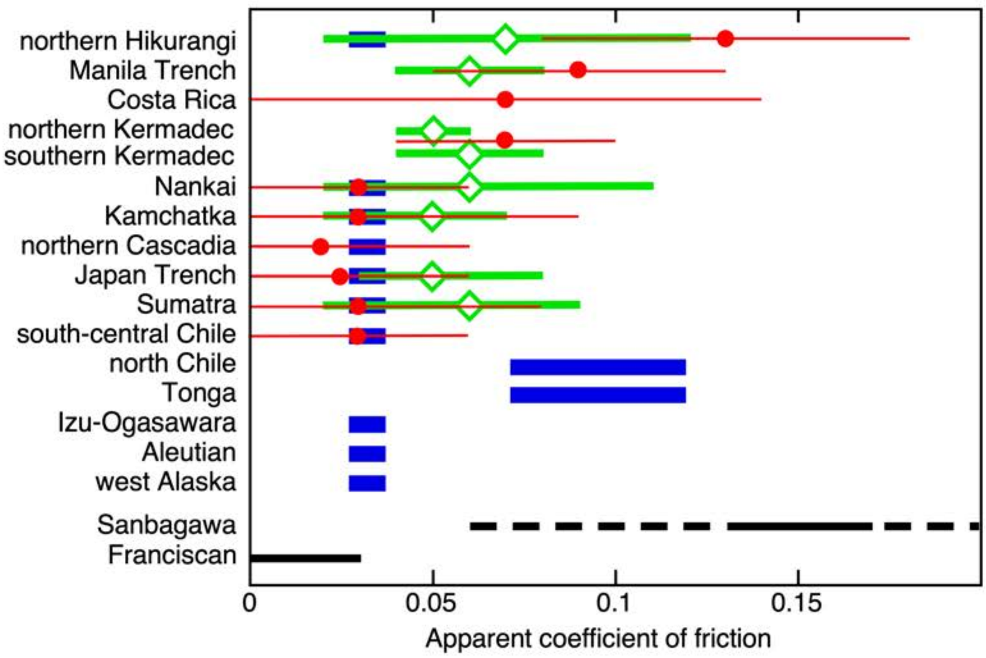

Ishii and Wallis, Figure 2
Single-column width

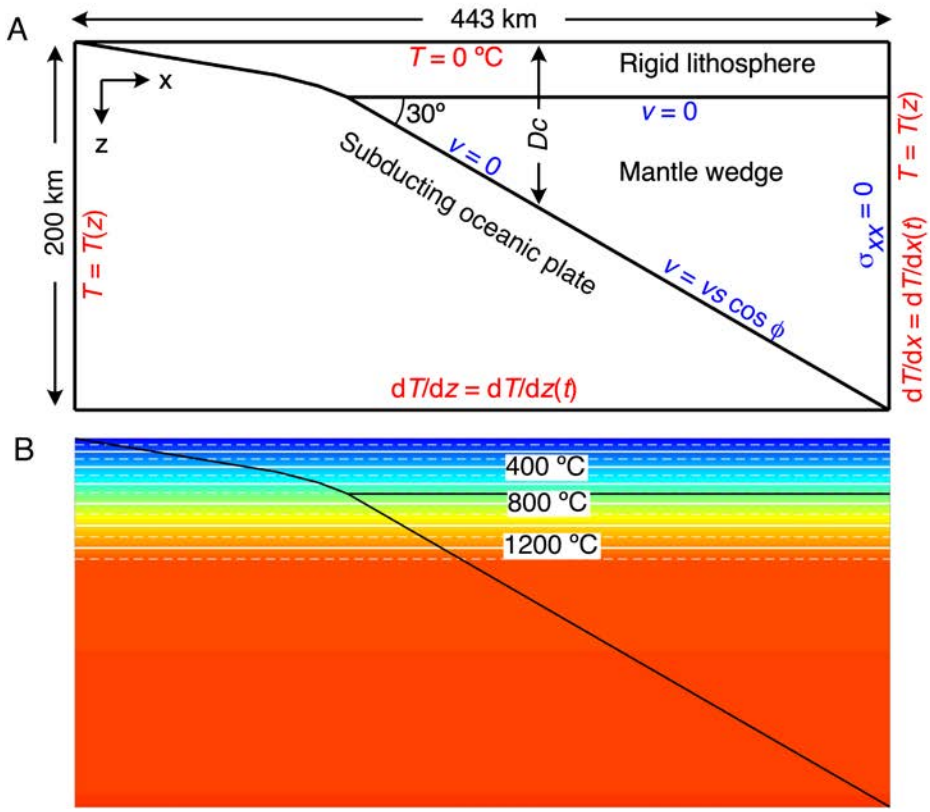

Ishii and Wallis, Figure 3
2-column width

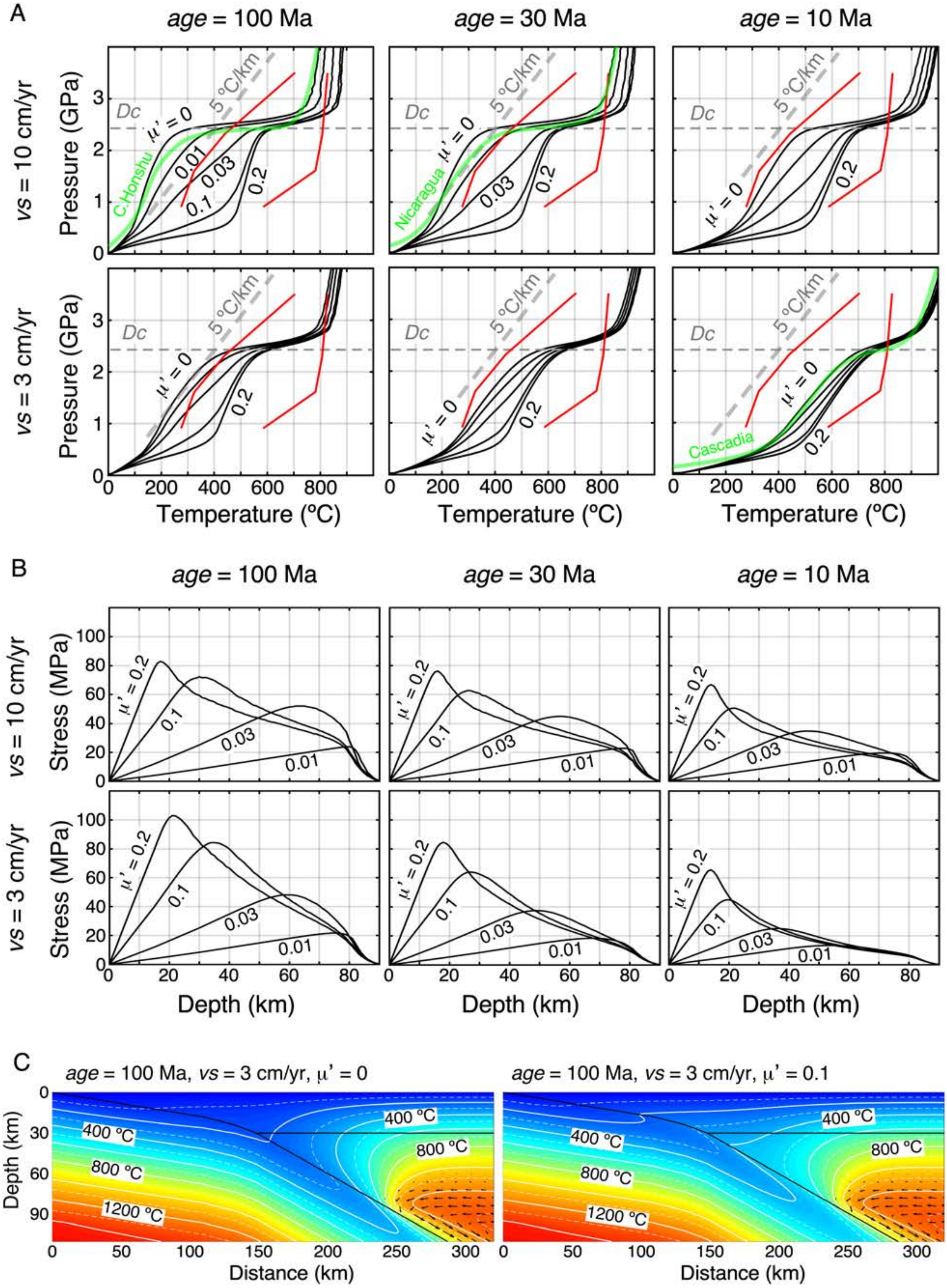

Ishii and Wallis, Figure 4
Single-column width

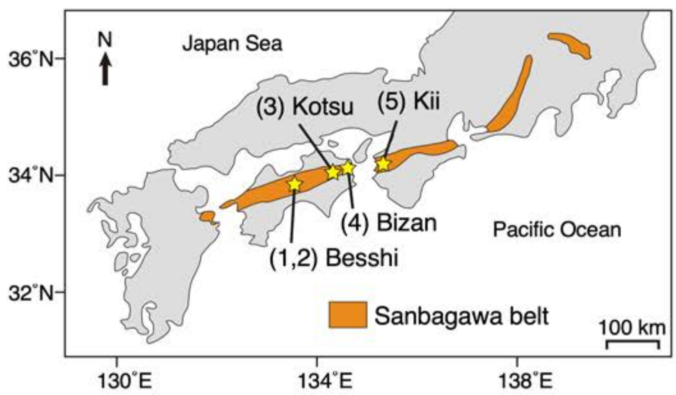

Ishii and Wallis, Figure 5
2-column width

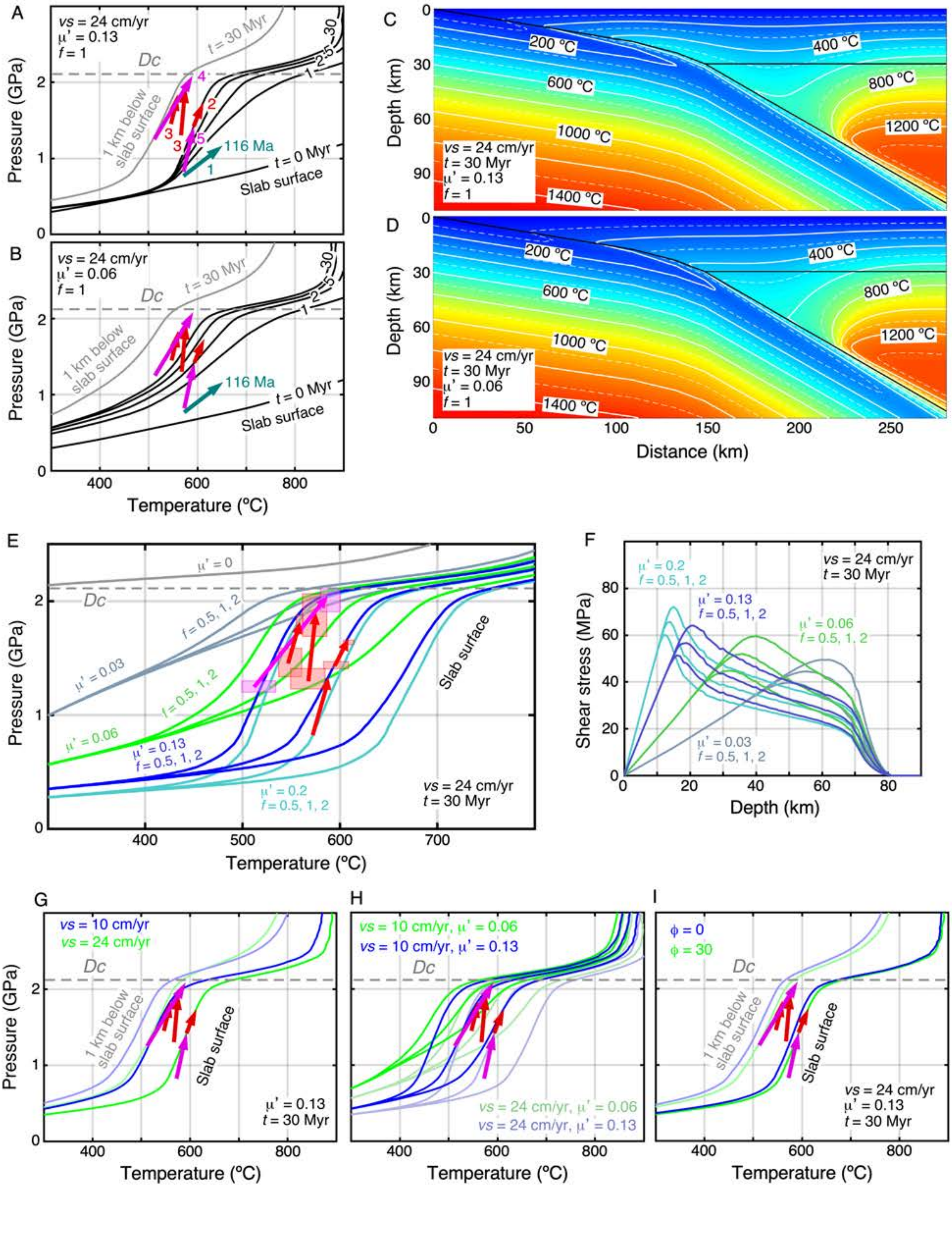

Ishii and Wallis, Figure 6
Single-column width

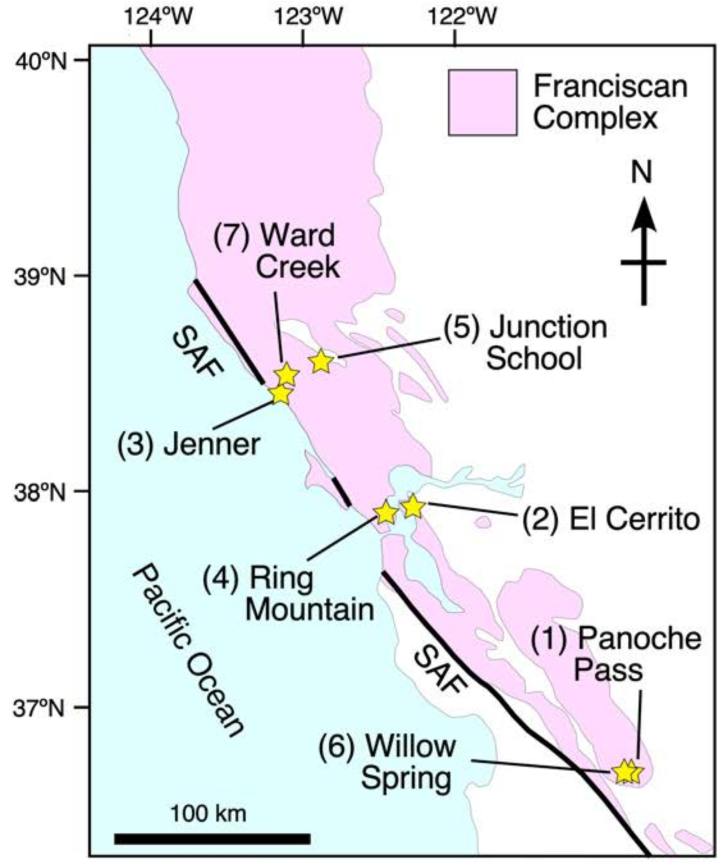

Ishii and Wallis, Figure 7
2-column width

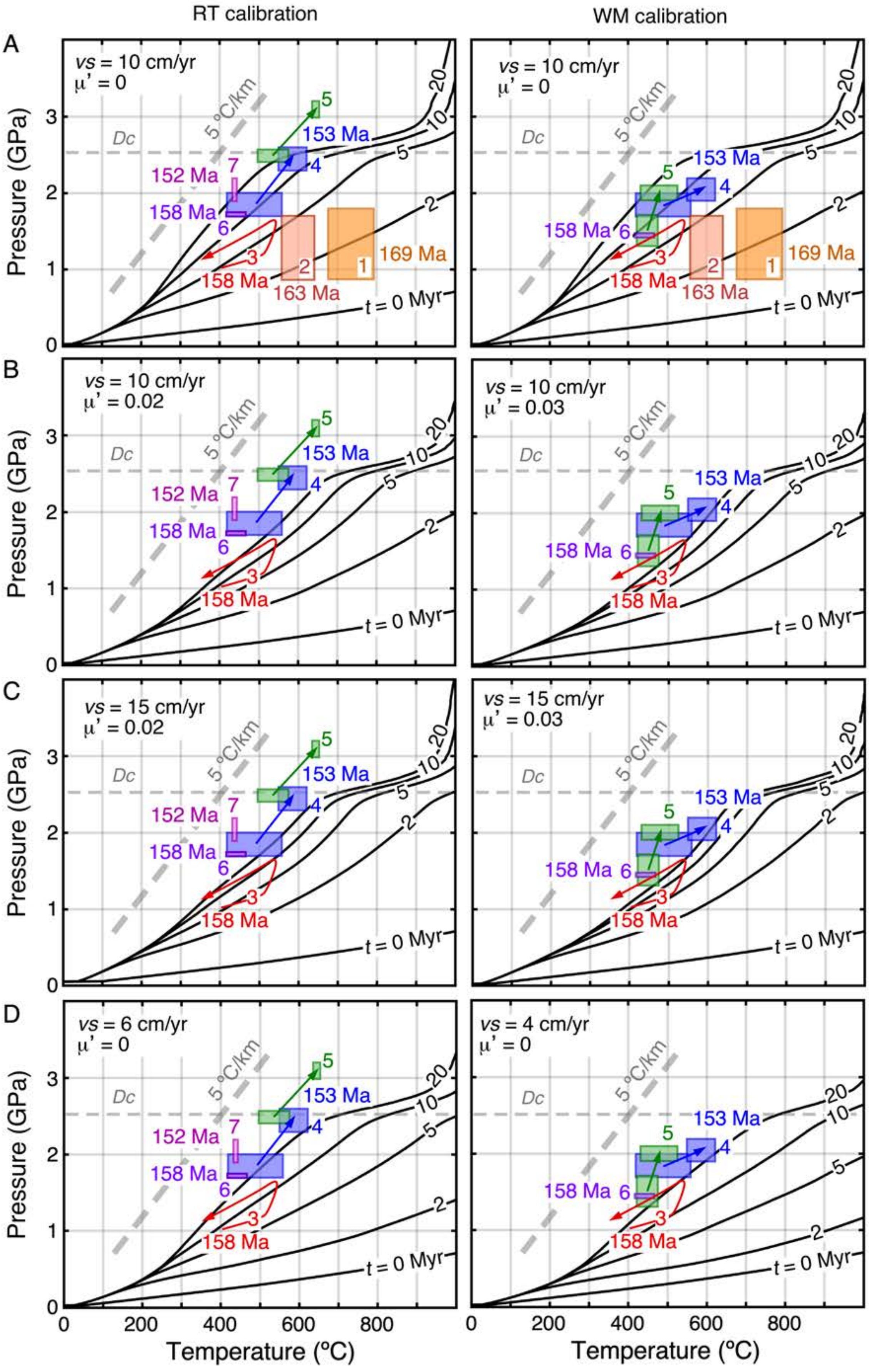

Ishii and Wallis, Figure 8
2-column width

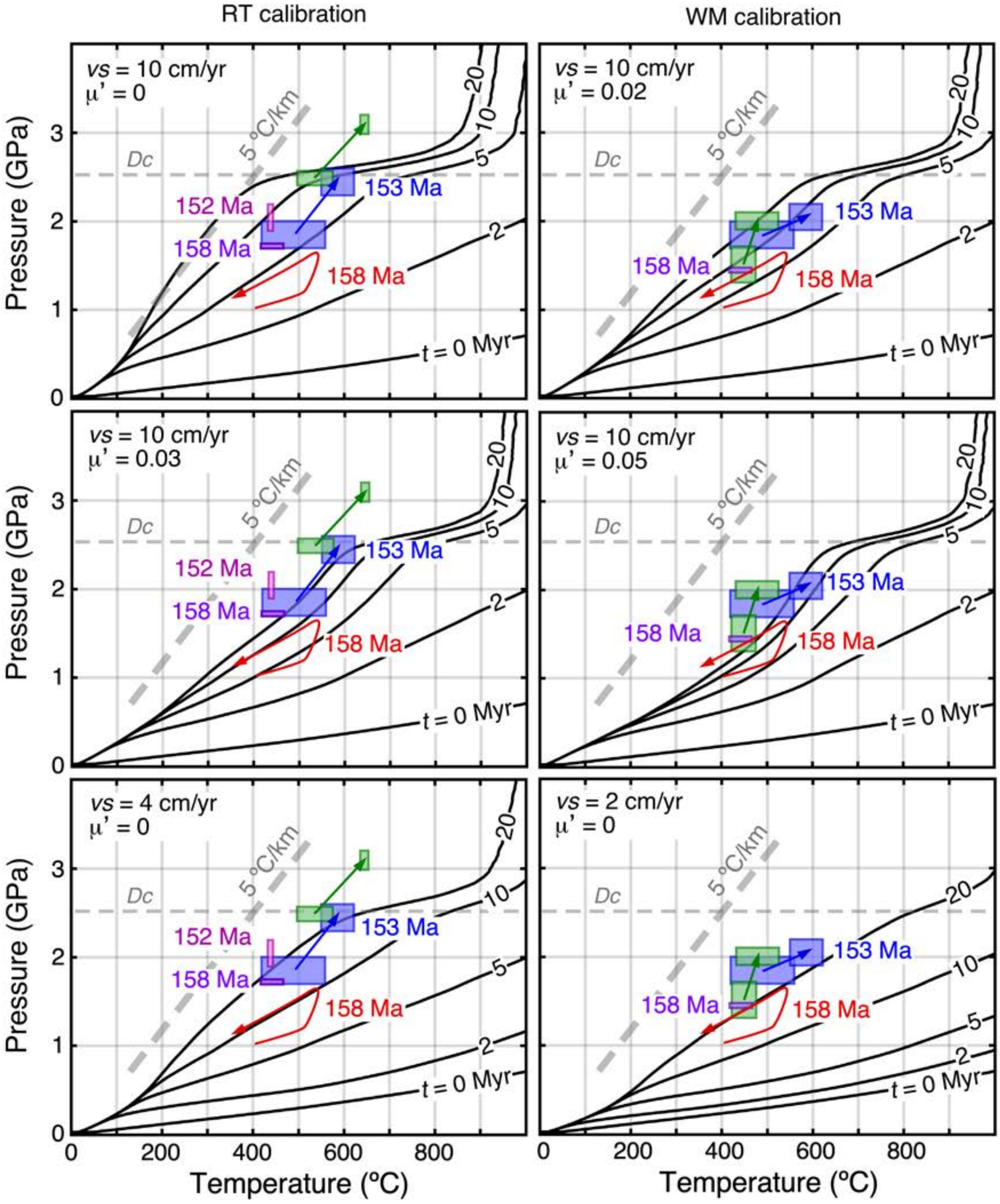

Ishii and Wallis, Figure 9
2-column width